Investigating the Effect of Different Boundary Conditions on the Identification of a Cavity Inside Solid Bodies

Mahmud Khodadad
Department of Mechanical Engineering,
Yazd University, Yazd, Iran
E-mail: khodadad@yazduni.ac.ir

Mohsen Dashti Ardakani*
Department of Mechanical Engineering,
Yazd University, Yazd, Iran
E-mail: mohsen_dashtiardakani@yahoo.com
*Corresponding author

Abstract: The effect of boundary conditions on the solution of the inverse problem of identifying the geometry and location of a cavity inside an elastic solid body using displacement measurements obtained from a tension test is investigated. The boundary elements method (BEM) coupled with the genetic algorithm (GA) and the conjugate gradient method (CGM) are implemented in this identification problem. A fitness function which is defined as the squared differences between the computed and measured displacements is minimized. The best initial guess of the unknown shape and location of the cavity is found by the GA, then this initial guess is used by the CGM to achieve convergence. The imposed boundary conditions, i.e. geometrical constrain and specified tractions are kept constant during all iterations. Certainly changes in the boundary conditions can be effective in the correct identification of the shape and location of the cavity. In this study the effect of different boundary conditions on the convergence is investigated and the best and the most suitable boundary conditions which results in the faster and more accurate convergence are found.

Reference: M. Khodadad and M. Dashti Ardakani, (2011) 'Investigating the Effect of Different Boundary Conditions on the Identification of a Cavity Inside Solid Bodies', Int J Advanced Design and Manufacturing Technology, Vol. 4/ No. 4 , pp. 9-17.

Biographical notes: M. Khodadad accomplished all his engineering studies in Mechanical Engineering in Michigan State University (MSU), USA 1990. He is currently working as Assistant Professor at the Department of Mechanical Engineering, Yazd University, Yazd. His current research interests include Implementing of Numerical Methods such as Finite Element Method (FEM) and Boundary Element Method (BEM) in Inverse Problems. **M. Dashti Ardakani** received his MSc in Mechanical Engineering from Yazd University, Iran 2005. After graduation, he has worked as Graduated Research Assistant (GRA) at Yazd University up to now. His current researches focus on Numerical Methods and New Global Optimization Techniques in Inverse Problems.

1   INTRODUCTION

Identification of the shape and location of inclusions, cavities and cracks inside solid bodies are among the most interesting problems in the field of engineering analysis.

Over the years different methods of identifying the internal structure of solid bodies mostly based on numerical techniques and experimental measurements has been proposed. Since iterative numerical techniques must be employed in these non-linear identification problems, to avoid remeshing of the whole domain after each iteration, the BEM which only needs boundary discretization is most suitable. It also allows us to use surface measurements which are important in the field of nondestructive evaluation [1].

The inverse elasticity problem coupled with the BEM has been used to detect defects in plane stressed body [2], nondestructive identification of cavities [3], the identification of geometric shape of inclusions inside infinite bodies [4], estimation of physical properties and size of a circular inclusion [5] and the physical properties and geometric shape of an inclusion using the GA and CGM coupled with the BEM [6].

Different local optimization algorithms are implemented in the inverse elasticity problem and the advantages and disadvantages of each algorithm has been addressed in [7].

The identification of the location, shape and elastic properties of an inclusion using boundary displacements measured from a tension test is investigated in [8]. The GA is used to find the best estimated initial guess of unknown parameters, and then the CGM is implemented to achieve fast and accurate convergence.

In all the investigations mentioned, the main purpose has been to introduce the inverse problem and estimate some unknown parameters related to the geometry or physical properties of inclusions, but none has investigated the effectiveness of different boundary conditions i.e. the geometric constraints and loading conditions employed in an experimental procedure and obtain surface displacement measurements.

In this study we will investigate many different geometric constraints, loading conditions and combination of these involved to find the optimum boundary conditions. The inverse elasticity similar to [8] is formulated. Four different geometric constraints combined with three different loading conditions to identify an elliptic shape cavity located at three different locations inside a solid body is investigated.

2   FORWARD PROBLEM STATEMENT

The solution of the forward elastostatics problem provides the displacement field given the governing equation, the boundary conditions, and the domain geometry. The displacement field for an isotropic, homogeneous, and linearly elastic body with neglected body force is governed by the Navier equation:

$$\left(\frac{1}{1-2\nu}\right)\frac{\partial^2 u_j}{\partial x_i \partial x_j} + \frac{\partial^2 u_i}{\partial x_j \partial x_j} = 0 \qquad (1)$$

where u_i is the component of the displacement in the ith coordinate direction, ν is Poisson's ratio. In a forward problem, the solution of this equation is typically sought subject to two possible boundary conditions:

Displacement conditions:

$$u_i = \bar{u}_i \qquad\qquad on\ \Gamma_u \qquad (2)$$

Traction conditions:

$$t_i = \sigma_{ij} n_j = \bar{t}_i \qquad\qquad on\ \Gamma_t \qquad (3)$$

where the overbar denotes a specified quantity, t_i is the component of the traction in the ith coordinate direction, and $\hat{n}$ is the outward drawn normal. The BEM solution of Eq. (1) subject to Eqs. (2) and (3) leads to the following boundary integral equation [9]:

$$c_{jk}^i u_k^i + \int_\Gamma t_{jk}^* u_k d\Gamma = \int_\Gamma u_{jk}^* t_k d\Gamma \qquad (4)$$

where the superscript i is used to denote the boundary point i, u_{jk}^* and t_{jk}^* are the fundamental displacement and tractions (Kelvin's solution), and the matrix c_{jk}^i is discussed and given in [9]. The domain is denoted by Ω and its boundary by Γ. Introducing boundary elements, Eq. (4) is discretized in the standard BEM form where the body forces are neglected as:

$$[H]\{U\} = [G]\{T\} \qquad (5)$$

If there is a cavity in the domain Ω, tractions free condition is specified on its boundary. Introducing the boundary conditions into the nodal displacement and traction vectors $\{U\}$ and $\{T\}$ and rearranging by taking known quantities to the right hand side and unknowns to the left, leads to a set of simultaneous linear equations of the form $[A]\{X\} = \{B\}$. These equations are solved by standard methods.

3 INVERSE PROBLEM STATEMENT

In the inverse problem the geometry and location of the cavity are unknown, but some of the unknown boundary data like displacements and/or tractions can be measured and employed as additional information necessary to estimate the unknown input parameters. A body that is known to contain a cavity with unknown location and shape is considered. Parameters which identify the location and the shape of the cavity are determined using the measurement of displacements on the portion of the boundary where tractions are prescribed. The following column matrices are introduced:

$[u_e]$: A column vector containing M measured boundary displacements.

$[u_c]$: A column vector containing the same M boundary displacements, computed using the BEM.

$[x]$: A column vector containing N unknown parameters which it is defined as:

$$[x] = [x_c, y_c, r_1, ..., r_n]^T \qquad (6)$$

x_c and y_c are the x-y coordinates of the center of the cavity and the r_i are the radial distance of n nodal locations on the cavity's boundary to center of cavity as shown in Fig. 1. The fitness function which is the squared differences between measured and computed displacements is:

$$f(\hat{x}) = \sum_{m=1}^{M} \left[u_c^m - u_e^m \right]^2 \qquad (7)$$

where «∧» denotes the estimated values of the unknown parameters.

In order to minimize the fitness function, the identification procedure is conducted in two stages. In the first stage the GA is employed to estimate the best initial guess of the unknown parameters, and then this initial guess is used in the second stage by the CGM to achieve fast and accurate convergence.

4 GENETIC ALGORITHM (GA)

The estimated initial guess of the shape of the cavity is assumed to be a circular, since it is the simplest shape with smooth boundary. Three parameters, i.e. x-y coordinates of the center of the circle and its radius is only needed to estimate the shape of the cavity.

Therefore, unknown parameters which are estimated using GA are defined as:

$$[x_G] = [x_{cg}, y_{cg}, r_g]^T \qquad (8)$$

In this investigation, the appropriate operators and the values of the GA parameters are obtained by examining different choices of operators and parameters and many trial and error runs.
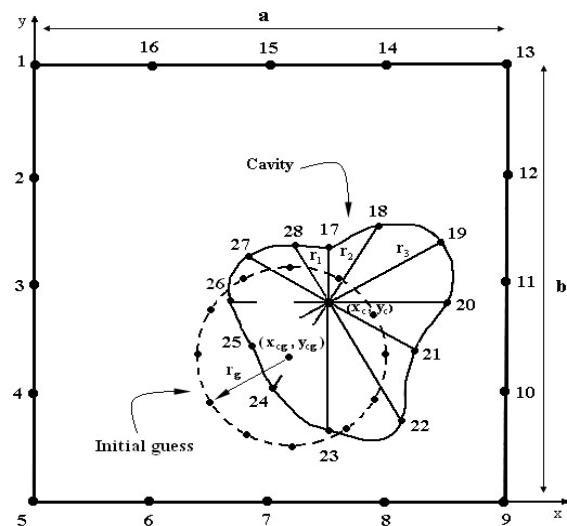
Fig. 1   Geometric parameters and problem modeling

So the *Roulette Wheel* is chosen as the selection operator. The *Rank* is chosen as the fitness scaling operator and also one *Elite Count* is used [10]. But since the geometric parameters must be within a specified range, the reproduction operators must be simulated specifically in order to get a correct solution to this problem as follows:

Initial Population: The initial population should be chosen such that all the unknown parameters represented by Eq. (8) are represented. The first two genes do not have any limit in their values. But the radius should be such that the boundary of the cavity remains within the domain of the problem. Therefore if the cavity is assumed to be inside a rectangular domain with dimensions of a and b as shown in Fig.1, then the radius should be bounded as:

$$\Pr(x_{cg}, y_{cg}, r_g)$$

$$\{$$

$$return \begin{pmatrix} (0 < x_{cg} + r_g \sin\theta_i < a) & and \\ (0 < y_{cg} + r_g \cos\theta_i < b) & \end{pmatrix}; \qquad (9)$$

$$\}$$

If the radius is within the above limits, it will be chosen as the candidate answer; otherwise another random value for radius will be tested. The function *Fr* takes the *x-y* coordinates of the center point and gives the proper radius, as follows:

$$Fr\left(x_{cg}, y_{cg}\right)$$
$$\{$$
$$do$$
$$\{$$
$$\quad r_g = Rnd\left(0,1\right); \tag{10}$$
$$\quad while \ \left(not \ \Pr(x_{cg}, y_{cg}, r_g)\right)\}$$
$$\quad return \ \left(r_g\right);$$
$$\}$$

The function IP for any x-y values inside the rectangular domain, gives proper initial population as follows:

$$IP\left(x_{cg}, y_{cg}\right)$$
$$\{$$
$$\quad x_{cg} = Rnd\left(0,a\right);$$
$$\quad y_{cg} = Rnd\left(0,b\right); \tag{11}$$
$$\quad r_g = Fr\left(x_{cg}, y_{cg}\right);$$
$$\quad return \left(\left[x_G\right] = \left[x_{cg}, y_{cg}, r_g\right]\right);$$
$$\}$$

Crossover Operation: The crossover operator is chosen according to the following criteria:

$$Crossover \ \left(\left[x_G\right], \left[x_G'\right]\right) \qquad \begin{array}{l} \left[x_G\right] = \left[x_{cg}, y_{cg}, r_g\right] \\ \left[x_G'\right] = \left[x_{cg}', y_{cg}', r_g'\right] \end{array}$$
$$\{$$
$$\quad \left[Child_{xx'}\right] = \left[x_G\right] + R \times \left(\left[x_G'\right] - \left[x_G\right]\right); \tag{12}$$
$$\quad while \ \left(not \ \Pr\left(\left[Child_{xx'}\right]\right)\right)$$
$$\quad return \ \left(\left[Child_{xx'}\right]\right);$$
$$\}$$

where **R** is a random vector with dimension equal to the number of parameters or genes. It does not have any limit for the first two genes, but after the second gene, i.e. the radius of the circle, this random number must satisfy the geometric limitations.

An important factor in crossover operator is the method of defining crossover fraction (p_c). It gets a value between 0 and 1. With regard to this problem and the

nature of the unknown parameters, p_c is set equal to 0.8.

Mutation Operation: The mutation operator is very effective in finding the absolute optimum point without getting stock in local optima. The uniform mutation operator is considered for the first two genes, but for the third gene, it must satisfy as follows:

$$Mutation\left(\left[x_G\right], p_m\right) \qquad \left[x_G\right] = \left[x_{cg}, y_{cg}, r_g\right]$$
$$\{$$
$$\quad if \ \left(Rnd(0,1) < p_m\right);$$
$$\quad x = Rnd(0,a)$$
$$\quad if \ \left(Rnd(0,1) < p_m\right); \tag{13}$$
$$\quad y = Rnd(0,b)$$
$$\quad if \ \left(Rnd(0,1) < p_m \ and \ \Pr\left(x_{cg}, y_{cg}, r = r(a,b)\right)\right)$$
$$\quad return \ \left(\left[x_G\right]\right);$$
$$\}$$

p_m is called the mutation rate and is set equal to 0.01.

5 CONJUGATE GRADIENT METHOD (CGM)

CGM is based on minimizing the fitness function i.e. Eq. (7). To minimize this function we need the direction of descent $p^k(x)$ and the search step size β^k in the following equation [11]:

$$\hat{x}^{k+1} = \hat{x}^k + \beta^k p^k(\hat{x}) \tag{14}$$

where $k = 1,...,iTer_{CGM}$ and $iTer_{CGM}$ is the maximum number of iterations in the CGM. The direction of descent is given by:

$$p^k(\hat{x}) = -g^k(\hat{x}) + \gamma^k p^{k-1}(\hat{x}) \tag{15}$$

where $g^k(\hat{x})$ are gradient directions at iteration k. According to *Polack-Ribiere* [11] the conjugate coefficients γ^k are:

$$\gamma^k = \frac{(g^{k+1} - g^k)^T g^{k+1}}{(g^k)^T g^k} \tag{16}$$

where $\gamma^0 = 0$. In cases where algorithm does not converge after n step, γ gets the value of zero. The gradient function $g^k(\hat{x})$ is computed using the finite difference method as follows:

$$g_{ij}(\hat{x}) = \frac{\partial f_i(\hat{x})}{\partial \hat{x}_j} = \frac{f_i(x_1,..,x_j+\delta x_j,..,x_N)-f_i(x_1,..,x_j,..,x_N)}{\delta x_j}$$ (17)

$$\delta x_j = 10^{-4} \times x_j$$

To compute the search step size β^k, using Eq. (7), the function $f(\hat{x})$ in step $k+1$ could be written as:

$$f(\hat{x}^{k+1}) = \sum_{m=1}^{M} \left[u_c^m(\hat{x}^k + \beta^k p^k) - u_e^m \right]^2$$ (18)

using Taylor series, it is written in the form:

$$f(\hat{x}^{k+1}) = \sum_{m=1}^{M} \left[u_c^m(\hat{x}^k) - \beta^k \Delta u_c^m(p^k) - u_e^m \right]^2$$ (19)

where $u_c^m(\hat{x}^k)$ is computed by solving the direct problem using BEM. The search step size β^k is determined by minimizing the function given by Eq. (19) with respect to β^k. The following expression results:

$$\beta^k = \frac{\sum_{m=1}^{M} \left[u_c^m(\hat{x}^k) - u_e^m \right] \Delta u_c^m(\hat{x}^k)}{\sum_{m=1}^{M} \left[\Delta u_c^m(\hat{x}^k) \right]^2}$$ (20)

where Δu_c^m needed to compute β^k is computed by solving direct problem with $\Delta \hat{x}^k = p^k$.

6   ANALYSIS MODEL

A computer program is developed in order to simulate numerically the estimation of the shape and location of a cavity hidden inside a solid body, using measured boundary displacements. The effects of different choices of boundary conditions are investigated by first simulating measured displacements data. The direct problem with known location and shape of the cavity along with specified boundary conditions is solved for the unknown boundary displacements.

A $(1 \times 1 m^2)$ square shaped steel grid with $E_s = 210\ GPa$ and $\nu = 0.3$ is used throughout the investigation. The cavity is assumed to have an elliptic shape. The outer boundary is divided into 16 linear elements and cavity's boundary is divided into 12 elements as shown in Fig. 1.

Stopping criteria for the GA is determined by generations that specify the maximum number of iterations in the GA. With population size equals 200,

generation is considered 50. Stopping criteria for the CGM is determined after 100 iterations. The reason for selecting these stopping criteria is based on our knowledge of the characteristics of the real parameters and by playing with their values and by trial and error. These numbers are appropriate since they cause GA and CGM to converge and give accurate results with less computational time and are kept constant throughout the investigation. More details of implementing GA and CGM could be found in [12].

An error function is defined as:

$$\% err = \frac{\sum_{n=1}^{N} \left| \frac{x_{act}^n - x_{ext}^n}{x_{act}^n} \right|}{N} \times 100$$ (21)

where x_{act} and x_{est} are the actual and estimated values of the unknown parameters respectively and N is the number of unknown parameters. The accuracy of the results is the average value obtained from 10 different runs.

Geometric constraints (GC): Four different geometric constraints are considered:

a. Fixed support at the bottom boundary as shown in Fig. 2(a).

b. Rail support at the bottom boundary except at one point where pin support is specified as shown in Fig. 2(b).

c. One pin support at the bottom and one rail support at the top as shown in Fig. 2(c).

d. Four rail support at the four side of the body as shown in Fig. 2(d).

Loading conditions (LC): Three different loading conditions are considered. It should be mentioned that all the traction vectors are applied normal to the corresponding boundaries as follows:

a. Tractions are only applied at the top and bottom side, Fig. 3(a).

b. Tractions are only applied at the left and right side, Fig. 3(b).

c. Tractions are applied at all four sides, Fig. 3(c).

It should be noted that at a node, traction vectors are applied in the direction in which there is no geometric constraint in that direction.
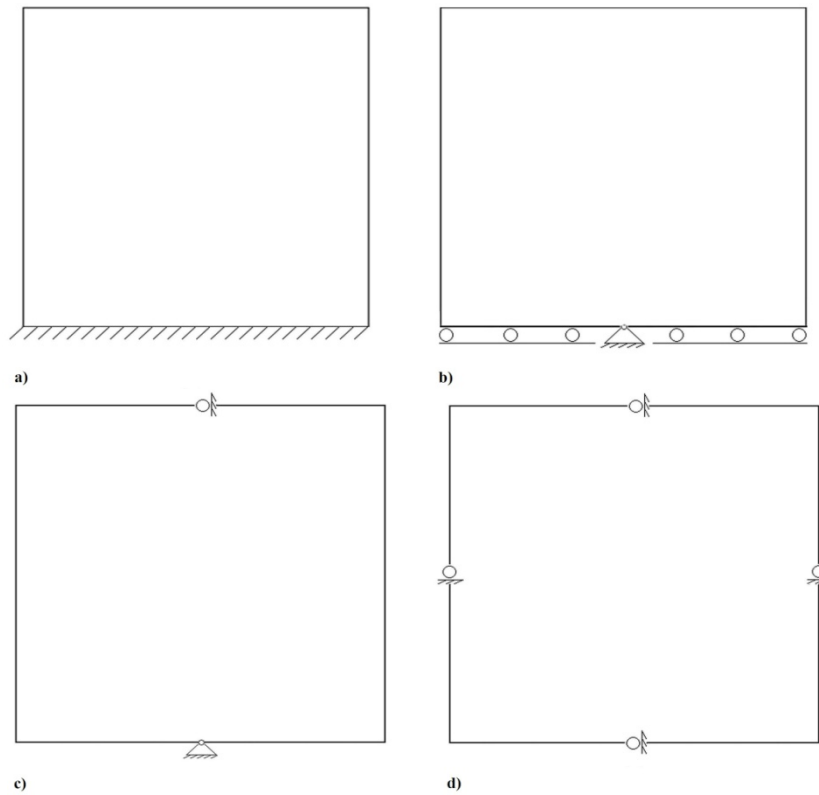
Fig. 2   Geometric constraints
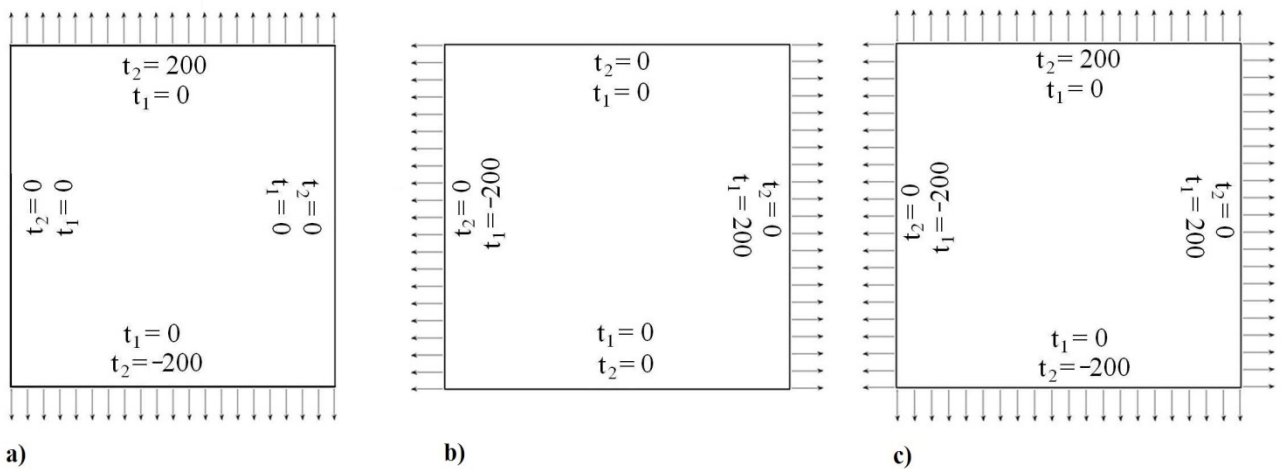
Fig. 3   Loading conditions

Cavity location: Along with different combination of the geometric constrains and loading conditions, three different locations of the elliptic shape cavity represented by equation $9x^2 + 36y^2 = 1$ is considered as:

1- The cavity is located at the center of the body at point (0.5,0.5) i.e. such as horizontal ellipse represented by H.

2- The cavity is located at the bottom right corner of the body at point (0.8,0.3) whose semi-axes are rotated with respect to horizontal axis by 90° i.e. such as vertical ellipse represented by V.

3- The cavity is located at the top left corner of the body at point (0.3,0.7) whose semi-axes are rotated with

respect to horizontal axis by -45° i.e. such as an oblique ellipse represented by O.

7   RESULTS

According to the four geometric constraints (GC) and three different loading conditions (LC) and three different locations of the cavity, 36 different combinations of these cases are defined and investigated. The percent cases which have resulted in complete convergence along with %err defined by Eq. (20) is presented in Table 1.

Figure 4 through Fig. 7 are sample figures based on the results represented in Table 1 with asterisk marked.

Table 1   Percent error obtained from the 36 different combinations of geometric constrains, loading conditions and cavity location cases

LC Type ►	(a)			(b)			(c)		
GC Type ▼	H	V	O	H	V	O	H	V	O
(a)	9.1316	*1 8.8010	7.5980	1.4397	11.1933	*2 5.0804	*3 16.5739	7.5341	3.6923
(b)	*4 8.8138	5.5905	7.4437	2.2226	*5 10.3680	7.4901	1.8723	11.2195	*6 5.0879
(c)	5.2590	4.2677	*7 9.1730	*8 2.2353	6.2689	6.5697	6.1830	*9 3.0706	6.8379
(d)	6.7863	*10 4.4263	8.7523	1.9327	6.2417	*11 7.6063	*12 0.8822	3.4654	2.2492
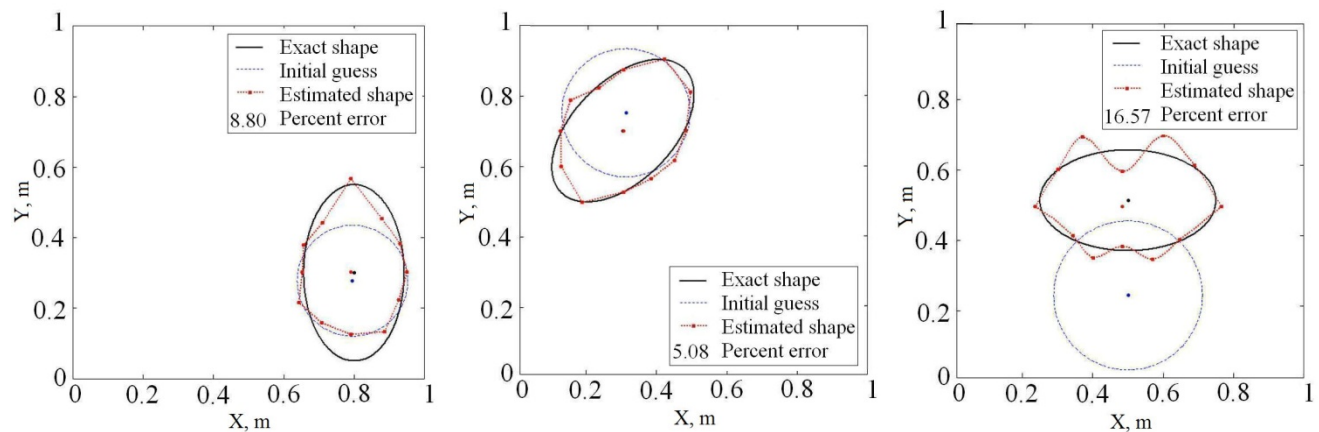
Fig. 4   Samples of converged results obtained from different combinations of geometric condition (a) and loading conditions (a,b,c) represented in *1,*2,*3
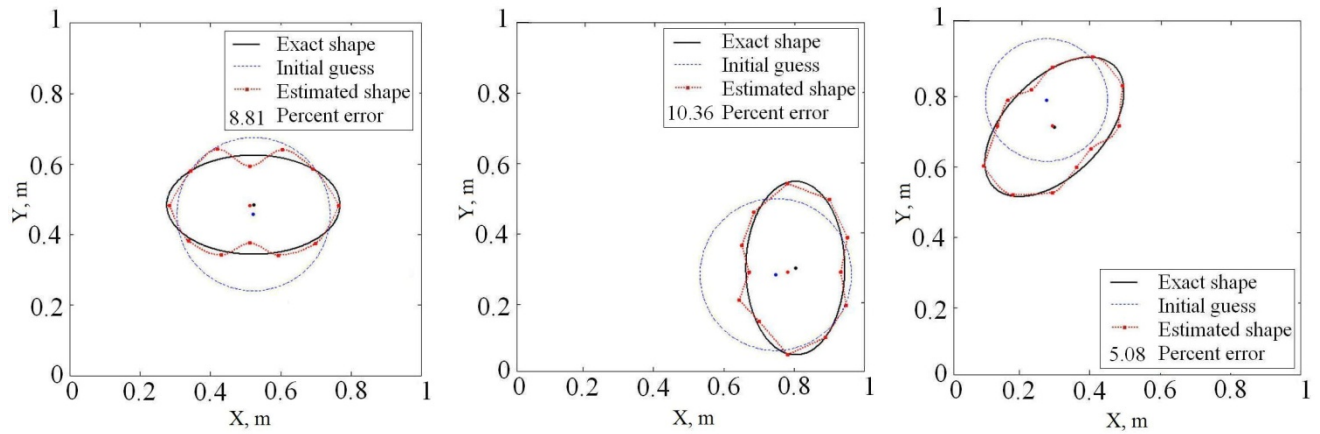
Fig .5   Samples of converged results obtained from different combinations of geometric condition (b) and loading conditions (a,b,c) represented in $*^4, *^5, *^6$
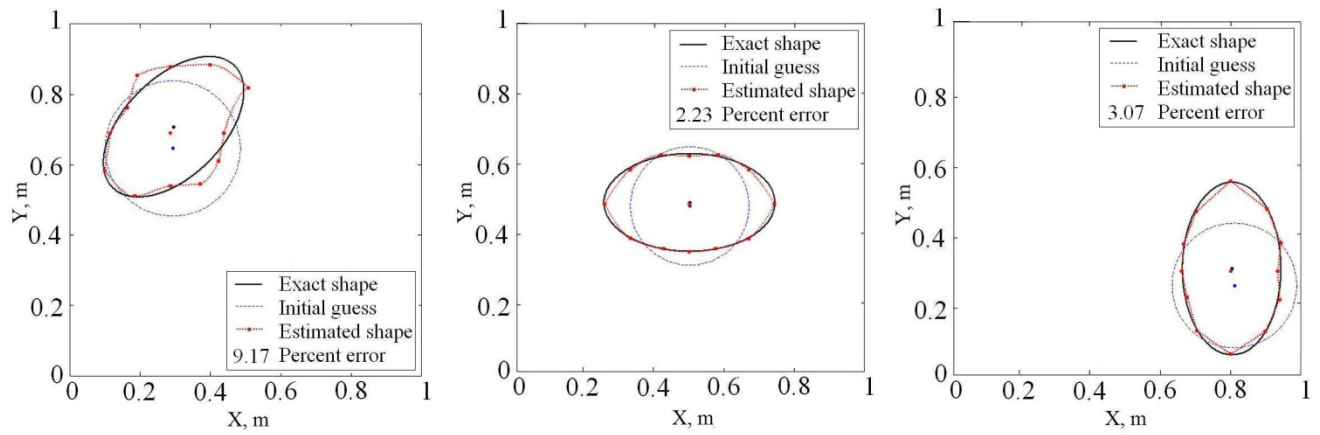
Fig. 6   Samples of converged results obtained from different combinations of geometric condition (c) and loading conditions (a,b,c) represented in $*^7, *^8, *^9$
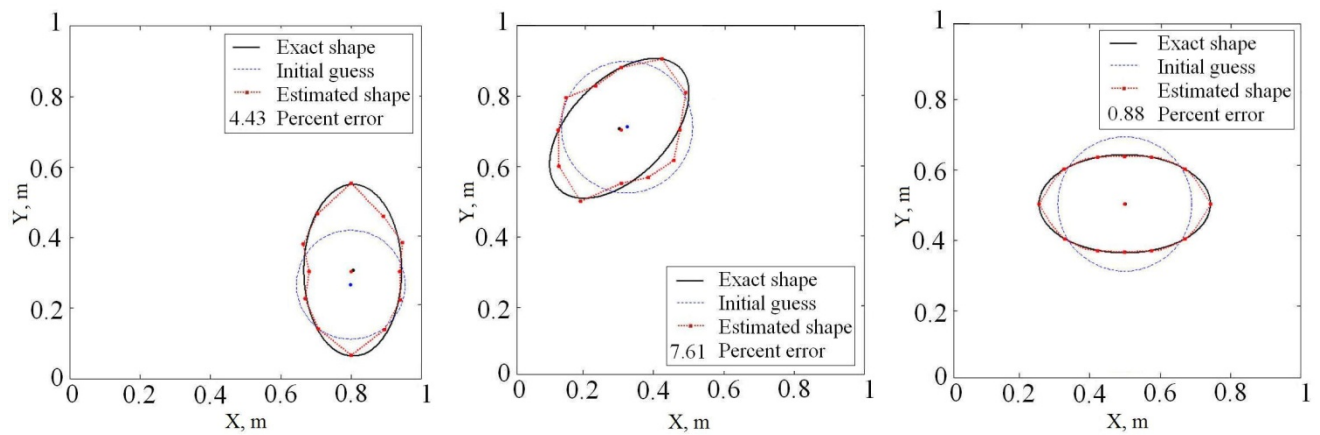
Fig. 7   Samples of converged results obtained from different combinations of geometric condition (d) and loading conditions (a,b,c) represented in $*^{10}, *^{11}, *^{12}$

8 CONCLUSIONS

Changing the boundary conditions and selection of the optimum geometric constraint and loading conditions to identifying the shape and location of a cavity located inside a solid body prove to be very effective in convergence to the correct results. The following observations and conclusions are also drawn form this investigation:

- By changing the boundary conditions, the best initial guess of the unknown parameters obtained from the GA would be different which leads to different convergence in the solution of the inverse problem.

- Displacements boundary conditions in comparison with traction boundary conditions, leads to less percent cases of convergence. The first geometric constraint shown by Fig. 2(a) leads to the worst convergence whereas for the boundary conditions shown by Fig. 2(b), (c), (d) results in better convergence.

- The position of the cavity has strong effect on the convergence. As the location of the cavity is at the center of the body, better convergence is obtained in comparison to the cases in which the cavity is located near the boundary.

- Among the four kinds of geometric constraints used in this investigation i.e. Fig. 2, the constraints shown in Fig. 2(d) leads to the best converged results, since all four sides of the body constrained statically. Also, it is preferable to apply load on all sides.

ACKNOWLEDGMENTS

REFERENCES

[1] Brebbia, C.A., and Dominguez, J., Boundary Elements, An Introductory Course, Computational Mechanics Publications, Southampton, 1989.

[2] Shin, S., and Moo Koh, H., "A Numerical Study on Detecting Defects in a Plane Stressed Body by System Identification," Nuclear Engineering and Design, Vol. 190, No. 1, 1999, pp. 17-28.

[3] Kassab, A. J., Moslehy, F. A. and Daryapurkar, A. B., "Nondestructive Detection of Cavities by an Inverse Elastostatics Boundary Element Method," Engineering Analysis with Boundary Elements, Vol. 13, 1994, pp. 45-55.

[4] Lee, H.S., Kim, Y.H, Park, C.J. and Park, H.W., "A New Spatial Regularization Scheme for the Identification of Geometric Shape of an Inclusion in Finite Body," International Journal for Numerical Method in Engineering, Vol. 46, No. 7, 1999, pp. 973-992.

[5] Khodadad, M., and Dashti-Ardakani, M., "Determination of the Location, Size and Mechanical Properties of an Elastic Inclusion Using Surface Measurements," Inverse Problems in Science and Engineering, Vol. 17, No. 5, 2009, pp. 591-604

[6] Lee, H.S., Park, CH. J., and Park, H. W., "Identification of Geometric Shapes and Material Properties of Inclusions in Two-Dimensional Finite Bodies by Boundary Parametrization," Computer Methods in Applied Mechanics and Engineering, Vol. 181, 2000, pp. 1-20.

[7] Rus, G. and Gallego, R., "Optimization Algorithms for Identification Inverse Problems with the Boundary Element Method," Engineering Analysis with Boundary Elements, Vol. 26, 2002, pp. 315- 327.

[8] Khodadad, M., and Dashti-Ardakani, M., "Inclusion Identification by Inverse Application of Boundary Element Method, Genetic Algorithm and Conjugate Gradient Method," American Journal of Applied Sciences, Vol. 5, No. 9, 2008, pp. 1158-1166.

[9] Khodadad-Saryazdi, M., "Characterization of the Interior of an Inhomogeneous Body Using Surface Measurements," Ph.D. Thesis, Michigan State University, East Lancing, Michigan, USA, 1990.

[10] Haupt, R.L., and Haupt, S.E., Practical Genetic Algorithms, 2nd ed., John Wiley and Sons, Inc, 2004.

[11] Luenberger, D.G., Linear and Nonlinear Programming, 2nd ed., Addison Wesley, 1989.

[12] Dashti-Ardakani, M., "Solving the Inverse Problem to Identify the Inclusion inside Materials, Using the Boundary Element Method and Genetic Algorithm," Master Thesis, Department of Mechanical Engineering, Yazd University, Yazd, Iran, 2006.